Genome-wide screening reveals producer-cell modifications that improve virus-like particle production and delivery potency

Diana Ly[1], Hyewon Jang[1], Adhiraj Goel[1], Arnav Singh[1], Aditya Raguram[1,2]*

[1] Whitehead Institute for Biomedical Research, Cambridge, MA, USA

[2] Merkin Institute for Transformative Technologies in Healthcare, Broad Institute of MIT and Harvard, Cambridge, MA, USA

* Correspondence: araguram@wi.mit.edu (A.R.)

Abstract

Engineered virus-like particles (eVLPs) are promising vehicles for transient delivery of gene editing agents. While extensive particle optimization has yielded efficient eVLPs, it remains underexplored whether engineering the cells used to produce eVLPs could further improve eVLP properties. We developed a genome-wide screening approach to systematically investigate how genetic perturbations in producer cells influence eVLP production. This approach generates eVLPs loaded with guide RNAs that identify the genetic perturbation in the cell that produced a particular particle; the abundance of each guide RNA in eVLPs therefore reflects how the corresponding genetic perturbation influences eVLP production or cargo loading. We applied this approach to identify several genes that regulate eVLP cargo expression and loading into particles during the production process. Leveraging these insights, we engineered producer cells that support increased eVLP cargo packaging and a 2- to 9-fold increase in eVLP delivery potency across several cargo, particle, and target-cell types in cultured cells and in mice. Our findings suggest the potential of producer-cell engineering as a useful strategy for improving the utility of eVLPs and related delivery methods.

Introduction

Methods for safely and efficiently delivering macromolecules into cells in culture (*in vitro*) and within the body (*in vivo*) are required for many therapeutic strategies, including gene editing therapies[1-5]. Recently, virus-like particles (VLPs) have emerged as promising vehicles for therapeutic macromolecule delivery that combine key advantages of canonical viral and non-viral delivery strategies[1,6]. In typical VLPs, viral scaffold proteins are used to package and deliver cargo proteins, ribonucleoproteins (RNPs), or mRNAs instead of viral genetic material, which leads to transient cargo delivery into recipient cells[1,6]. Several VLP-based delivery methods have proven particularly effective for gene editing applications[7-23] and offer an ideal combination of efficient on-target editing, minimal off-target editing, and programmable cell-type targeting capabilities. Current state-of-the-art VLPs, including engineered VLPs (eVLPs)[7,8,22], have achieved efficient *in vitro* gene editing in primary human cells and therapeutic *in vivo* gene editing in the mouse liver and retina, highlighting the utility of eVLP delivery for research and potential therapeutic applications.

While extensive engineering of eVLP components and particle architectures has afforded efficient eVLPs[7,8,22], further improvements to eVLP properties are still required to maximize their prospects for clinical translation. In particular, improving eVLP cargo packaging per particle or overall particle yield from the eVLP production process would enable more efficient gene editing with lower eVLP doses and simplify the production of eVLPs for large-scale studies. Standard methods for producing eVLPs involve the use of human producer cells to express eVLP components and assemble functional particles[7,8,22], suggesting that producer cells likely play an important role in the eVLP production process. However, previous studies have focused solely on particle engineering to improve eVLP properties, and none have explored whether producer-cell engineering could improve eVLP properties beyond what can be achieved through particle engineering alone. In this study, we systematically investigated how genetic perturbations in producer cells influence eVLP production and applied our findings to engineer producer cells that support improved eVLP production and delivery potency.

Results

Genome-wide screening reveals producer-cell perturbations that influence eVLP production

We began by developing an unbiased genome-wide screening approach to identify genetic perturbations in producer cells that influence eVLP production (Fig. 1a). We envisioned a general scheme in which eVLP production is initiated from a pool of genetically perturbed producer cells. Each producer cell in this pool expresses a Cas9-based genome modifying agent and a single copy of a guide RNA (sgRNA) that directs the installation of a specific genetic perturbation into that particular cell (Fig. 1a). Because eVLPs package Cas9-based cargos, the perturbation-inducing sgRNA expressed in a given producer cell is also loaded into any particles produced by that particular cell (Fig. 1a). Therefore, the abundance of a particular sgRNA in eVLPs reflects how the corresponding genetic perturbation influences eVLP production or cargo loading: sgRNAs that are more abundant identify perturbations that increase eVLP production or cargo loading, while sgRNAs that are less abundant identify perturbations that decrease eVLP production or cargo loading (Fig. 1a).

We used this general approach to perform a genome-wide knockout screen for cargo-loaded eVLP production in Gesicle 293T producer cells, a standard cell line used for eVLP production[7,8,22]. We transduced producer cells at a low multiplicity of infection (MOI) with a lentiviral sgRNA library containing 98,077 unique sgRNAs targeting 19,707 genes across the human genome[24] (Extended Data Fig. 1a). Each vector in the library also encoded constitutive expression of Cas9 nuclease. After selecting for Cas9 expression and expanding the transduced cells to generate a pool of single-knockout producer cells, we initiated fourth-generation (v4) base editor (BE)-eVLP production from these cells (Extended Data Fig. 1a). Importantly, to initiate eVLP production, we only transfected plasmids encoding the expression of adenine base editor (ABE8e)-packaging v4-eVLP protein components: (1) the gag–ABE (capsid–cargo) fusion, (2) the Moloney murine leukemia virus (MMLV) gag–pro–pol polyprotein, and (3) the vesicular stomatitis virus G (VSV-G) envelope protein. No additional sgRNA-encoding plasmid was transfected, ensuring that all eVLPs produced from a given producer cell packaged cargo containing the specific knockout-inducing sgRNA that was already introduced into that producer cell by lentiviral transduction (Fig. 1a and Extended Data Fig. 1a).

89 Following eVLP production, we isolated RNA from purified eVLPs and compared
90 this eVLP-packaged RNA to cellular RNA that was isolated from the single-knockout
91 producer-cell pool immediately prior to eVLP production (Fig. 1a and Extended Data Fig.
92 1a). To compare sgRNA abundances across both populations, we subjected both RNA
93 pools to template-switching reverse transcription[25], which enabled amplification and
94 sequencing of the spacer sequence at the 5' end of each sgRNA molecule (Extended
95 Data Fig. 1b). sgRNAs that are more abundant in the eVLP-packaged RNA compared to
96 the producer-cell RNA identify gene knockouts that increase eVLP production or cargo
97 loading, while sgRNAs that are less abundant identify gene knockouts that decrease
98 eVLP production or cargo loading (Fig. 1a and Extended Data Fig. 1a).
99 By aggregating the results for all sgRNAs targeting the same gene into gene-level
100 phenotypes, we determined the effect of each producer-cell gene knockout on eVLP
101 production or cargo loading (Fig. 1b and Extended Data Fig. 1c). We observed that the
102 majority of gene knockouts did not substantially impact eVLP production or cargo loading,
103 some knockouts decreased eVLP production or cargo loading, and very few knockouts
104 increased eVLP production or cargo loading (Fig. 1b). These results are consistent with
105 a model in which there are more genes in producer cells that positively regulate eVLP
106 production than genes that negatively regulate eVLP production. Taken together, the
107 results of this genome-wide knockout screen illuminate the producer-cell determinants of
108 eVLP production and nominate several gene knockouts ("hits") that appear to strongly
109 impact eVLP production or cargo loading (Fig. 1b).
110
111 *Knockout of HUSH-associated genes negatively impacts eVLP sgRNA packaging and*
112 *delivery potency*
113 Next, we sought to characterize the gene knockouts that most strongly decreased
114 eVLP production or cargo loading. The three strongest negative hits from our screen—
115 *MPP8*, *TASOR*, and *MORC2*—are all associated with the human silencing hub (HUSH)
116 complex, which is responsible for epigenetically silencing intronless transgenes, including
117 retroviral elements[26,27]. We first individually validated each negative hit by measuring the
118 relative sgRNA abundance in eVLPs produced from *MPP8*-, *TASOR*-, or *MORC2*-
119 knockout cells (hereafter collectively referred to as HUSH-knockout cells) compared to

120 eVLPs produced from standard producer cells. To independently generate each knockout
121 cell line, we mimicked the screen conditions and transduced Gesicle cells with a lentiviral
122 vector encoding constitutive expression of Cas9 nuclease and an appropriate targeting
123 sgRNA, selected cells for Cas9 expression, and isolated a polyclonal population of Cas9-
124 edited cells (Extended Data Fig. 2a). To control for the effects of Cas9 expression and
125 Cas9 nuclease-mediated indel generation on producer cells, we also applied the same
126 procedure to generate modified Gesicle cells using a sgRNA targeting *AAVS1*, a human
127 safe harbor locus[28]. After knockout generation, we initiated v4 BE-eVLP production from
128 each cell line by transfecting plasmids encoding the expression of all required
129 components, including a sgRNA targeting the human *BCL11A* +58 enhancer locus[29]
130 (Extended Data Fig. 2a). We detected by RT-qPCR a 1.5- to 3.8-fold decrease in sgRNA
131 abundance in BE-eVLPs produced from HUSH-knockout cells compared to BE-eVLPs
132 produced from *AAVS1*-knockout cells (Fig. 2a), confirming the results of our screen.
133 Additionally, when we transduced HEK293T cells with a range of doses of purified BE-
134 eVLPs and measured adenine base editing efficiencies at the *BCL11A* +58 enhancer
135 target locus via high-throughput sequencing (Extended Data Fig. 2a), we observed that
136 BE-eVLPs produced from HUSH-knockout cells exhibited a 2.3- to 4.4-fold decrease in
137 *in vitro* delivery potency (EC_{50}) compared to BE-eVLPs produced from *AAVS1*-knockout
138 cells (Fig. 2b). These results indicate that knockout of HUSH-associated genes *MPP8*,
139 *TASOR*, or *MORC2* in producer cells negatively impacts eVLP production or cargo
140 loading.

141 We hypothesized that these HUSH-associated genes might impact eVLP
142 production or cargo loading by modulating the expression of the lentivirally integrated
143 Cas9 nuclease that was used to generate the gene knockouts. To test this hypothesis,
144 we measured the relative abundance of Cas9 mRNA or protein in each knockout cell line
145 by RT-qPCR or Western blot respectively. We observed a 5.4- to 29-fold increase in
146 cellular Cas9 mRNA expression and a 10- to 14-fold increase in Cas9 protein expression
147 in HUSH-knockout cells compared to *AAVS1*-knockout cells (Fig. 2c,d and Extended Data
148 Fig. 3a). These results suggest a model in which HUSH-associated gene products
149 natively silence lentivirally integrated Cas9 expression in *AAVS1*-knockout producer cells,
150 but in HUSH-knockout cells, Cas9 is no longer efficiently silenced (Extended Data Fig.

151 3b). Therefore, during eVLP production, excess Cas9 protein in HUSH-knockout producer
152 cells likely competes for sgRNA binding and prevents sgRNA molecules from efficiently
153 binding to gag–ABE, which ultimately decreases both sgRNA packaging into eVLPs and
154 eVLP delivery potency (Extended Data Fig. 3b). To further investigate this phenomenon,
155 we used v4 Cas9-eVLP transduction instead of Cas9/sgRNA lentiviral transduction to
156 generate HUSH-knockout Gesicle cells that lacked any integrated Cas9 transgene
157 (Extended Data Fig. 2b). Notably, we did not detect any change in sgRNA abundance by
158 RT-qPCR in BE-eVLPs produced from these Cas9-free HUSH-knockout cells compared
159 to standard producer cells (Extended Data Fig. 4a). These results suggest that, consistent
160 with our model above, both lentivirally integrated Cas9 expression and knockout of
161 HUSH-associated genes are required to decrease sgRNA abundance in eVLPs.
162 Collectively, these data and our proposed model rationalize the negative performance of
163 HUSH-associated gene knockouts in our screen.

164 Interestingly, we noticed that BE-eVLPs produced from Cas9-free HUSH-knockout
165 cells still exhibited a 2.6- to 3.9-fold decrease in delivery potency compared to BE-eVLPs
166 produced from standard Gesicle cells (Extended Data Fig. 4b), suggesting that some
167 eVLP property other than sgRNA abundance was negatively impacted due to Cas9-free
168 HUSH-associated gene knockout. We hypothesized that these HUSH-associated genes
169 might also modulate the expression of eVLP components from plasmids transfected
170 during the eVLP production process. To investigate this possibility, we performed
171 Western blots to quantify eVLP cargo (gag–ABE) expression in producer cells following
172 transfection of eVLP production plasmids, which revealed a 2.1- to 4.4-fold increase in
173 gag–ABE protein expression in HUSH-knockout cells compared to Gesicle cells
174 (Extended Data Fig. 4c, d). We reasoned that this increase in eVLP cargo expression
175 might disrupt the optimal eVLP component stoichiometry (gag–ABE:gag–pro–pol ratio),
176 which was previously found to be an important determinant of eVLP potency[8]. Indeed,
177 reducing the transfected gag–ABE:gag–pro–pol plasmid ratio from 25:75 to 10:90 or 5:95
178 restored the potency of BE-eVLPs produced from *MORC2*-knockout cells back to
179 standard levels (Extended Data Fig. 4e). These results indicate that the increase in eVLP
180 cargo expression in HUSH-knockout producer cells and corresponding disruption of the
181 optimal eVLP component stoichiometry can be counteracted simply by reducing the

182 amount of transfected eVLP cargo plasmid, thereby effectively restoring the optimal
183 stoichiometry. Altogether, our results reveal a previously unknown role for HUSH-
184 associated genes in modulating eVLP cargo expression in producer cells and highlight
185 the importance of optimizing eVLP cargo expression and component stoichiometry to
186 maximize eVLP potency.
187
188 *MAF1-knockout producer cells improve sgRNA packaging into eVLPs*
189 Next, we sought to characterize the gene knockouts from our screen that most
190 strongly increased eVLP production or cargo loading. The single strongest positive hit
191 from our screen was *MAF1*, a repressor of RNA Pol III transcription[30-32]. Because all
192 sgRNAs in our experiments were expressed from an RNA Pol III-transcribed U6 promoter,
193 we reasoned that knockout of *MAF1* in producer cells likely leads to increased sgRNA
194 transcription and loading into eVLP-packaged cargos (Fig. 3a).
195 To test this hypothesis, after generating *MAF1*-knockout Gesicle cells using v4
196 Cas9-eVLPs (Extended Data Fig. 2b), we initiated v4 BE-eVLP production from these
197 cells by transfecting plasmids encoding the expression of all required components. We
198 detected by RT-qPCR a 2-fold increase in sgRNA abundance in BE-eVLPs produced
199 from *MAF1*-knockout cells compared to BE-eVLPs produced from standard Gesicle cells
200 (Fig. 3b). Additionally, we observed that BE-eVLPs produced from *MAF1*-knockout cells
201 were produced at similar particle titers and packaged similar numbers of BE cargo
202 proteins per particle compared to BE-eVLPs produced from standard Gesicle cells (Fig.
203 3c and Extended Data Fig. 5a), suggesting that the use of *MAF1*-knockout cells increases
204 sgRNA packaging alone without affecting protein packaging or particle yield. Collectively,
205 these data confirm our knockout screen results and indicate that *MAF1*-knockout
206 producer cells support increased sgRNA loading into eVLPs.
207
208 *MAF1-knockout producer cells support improved eVLP delivery potency in cell culture*
209 *and in mice*
210 Because increased sgRNA loading leads to an increased number of active RNP
211 cargo molecules packaged into eVLPs (Fig. 3a), we reasoned that BE-eVLPs produced
212 from *MAF1*-knockout cells should exhibit increased delivery potency compared to BE-

213 eVLPs produced from standard Gesicle cells. Encouragingly, we observed that v4 BE-
214 eVLPs produced from *MAF1*-knockout cells exhibited a 2.5-fold increase in delivery
215 potency (EC_{50}) at the *BCL11A* +58 enhancer locus in HEK293T cells compared to v4 BE-
216 eVLPs produced from standard Gesicle cells (Fig. 4a). v4 BE-eVLPs produced from
217 *MAF1*-knockout cells also exhibited a 2.2- and 2.1-fold increase in delivery potency at the
218 *GAPDH* and *HIRA* genomic loci in HEK293T cells, respectively (Fig. 4b, c), indicating that
219 the eVLP potency improvement conferred by the use of *MAF1*-knockout producer cells is
220 not restricted to any particular sgRNA sequence or target genomic locus. Additionally, we
221 assessed whether the use of *MAF1*-knockout producer cells could also improve the
222 delivery potency of the more recently developed v5 BE-eVLPs, which use laboratory
223 evolved capsid proteins that were optimized to improve BE RNP cargo packaging[22]. We
224 observed that v5 BE-eVLPs produced from *MAF1*-knockout cells exhibited a 2.2- to 9.1-
225 fold increase in delivery potency compared to v5 BE-eVLPs produced from standard cells
226 across six distinct target genomic loci in mouse Neuro-2a cells (Fig. 4d–i). Together,
227 these results indicate that the increased sgRNA packaging in BE-eVLPs produced from
228 *MAF1*-knockout cells leads to corresponding improvements in eVLP delivery potency *in*
229 *vitro*.
230 To further explore the utility of *MAF1*-knockout producer cells, we investigated
231 whether their use could also improve *in vivo* eVLP delivery efficiencies. We produced v5
232 BE-eVLPs targeting the *Pcsk9* exon 1 splice donor[8,33] using either standard or *MAF1*-
233 knockout Gesicle cells, and we injected these BE-eVLPs retro-orbitally into adult mice at
234 a low, sub-saturating eVLP dose (Fig. 4j). We observed that v5 BE-eVLPs produced from
235 *MAF1*-knockout cells achieved 19.4% average *in vivo* base editing at the *Pcsk9* locus in
236 bulk liver tissue, while v5 BE-eVLPs produced from standard cells administered at the
237 same dose only achieved 12.6% bulk liver editing (Fig. 4j, $P = 0.0365$, two-sided unpaired
238 *t* test). Collectively, these data indicate that *MAF1*-knockout producer cells support
239 improved eVLP potency across different target genomic loci and target-cell types both *in*
240 *vitro* and *in vivo*, demonstrating the benefits of using *MAF1*-knockout cells instead of
241 standard cells for eVLP production.
242

243 *MAF1-knockout producer cells support improved delivery potency across various cargo*
244 *and particle types*

245 We next sought to further evaluate the ability of *MAF1*-knockout producer cells to
246 support improved eVLP production and potency in other various contexts. First, we
247 assessed whether *MAF1*-knockout producer cells could improve the potency of eVLPs
248 that package different Cas9-based RNP cargos. We observed that v4 eVLPs packaging
249 either ABE8e-SpCas9-NG[34], TadCBEa[35], or Cas9 nuclease cargos exhibited a 2.0- to
250 2.5-fold improvement in potency in HEK293T cells when produced from *MAF1*-knockout
251 cells compared to Gesicle cells (Extended Data Fig. 5b–f).

252 Second, we investigated whether *MAF1*-knockout producer cells could also
253 improve the performance of non-eVLP delivery vehicles, such as the recently reported
254 "engineered nucleocytosolic vehicles for loading of programmable editors" (ENVLPE$^+$)[10].
255 Interestingly, we observed that ABE8e-packaging ENVLPE$^+$ particles produced from
256 *MAF1*-knockout cells also exhibited a 2.2-fold increase in potency in HEK293T cells
257 compared to the same particles produced from Gesicle cells (Extended Data Fig. 5g).
258 Notably, even though ENVLPE$^+$ particles differ substantially from eVLPs in their viral
259 scaffold (HIV versus MMLV) and cargo loading mechanism (aptamer-containing sgRNA
260 loading versus gag–cargo fusion loading), both ENVLPE$^+$ particles and eVLPs
261 demonstrated nearly identical improvements in potency when produced from *MAF1*-
262 knockout cells compared to Gesicle cells (Extended Data Fig. 5g, h).

263 Third, we explored whether knockout of *MAF1* could improve eVLP production
264 from HEK293T/17 cells, another cell line that is commonly used for viral vector
265 production[8,22,36]. Following the generation of *MAF1*-knockout HEK293T/17 cells using v4
266 Cas9-eVLPs, we observed that v4 BE-eVLPs produced from *MAF1*-knockout
267 HEK293T/17 cells exhibited a 2.5-fold increase in *in vitro* delivery potency compared to
268 those produced from unmodified HEK293T/17 cells (Fig. 4k). These results indicate that
269 the improvements conferred by *MAF1* knockout appear to be generalizable beyond the
270 specific cell line in which our knockout screen was conducted. Taken together, our
271 findings demonstrate that knockout of *MAF1* in producer cells yields remarkably general
272 and consistent improvements in VLP delivery potency across eVLP cargo types, particle
273 types, and producer-cell lines.

274

275 **Discussion**

276 In this study, we developed a general genome-wide screening approach to
277 comprehensively evaluate how genetic perturbations in producer cells influence eVLP
278 production. Using this approach, we identified the HUSH epigenetic silencing complex
279 and the RNA Pol III repressor MAF1 as key regulators of eVLP protein and sgRNA cargo
280 expression, respectively. Leveraging these insights, we engineered *MAF1*-knockout
281 producer cells and demonstrated that these modified producer cells support a 2- to 9-fold
282 increase in eVLP delivery potency across several cargo, particle, producer-cell, and
283 target-cell types.

284 We anticipate that the use of *MAF1*-knockout cells instead of standard producer
285 cells will advance the utility of VLP delivery in several ways. For one, eVLPs produced
286 from *MAF1*-knockout cells exhibit increased sgRNA packaging and increased delivery
287 potency both in cell culture and in mice compared to standard eVLPs (Fig. 4), suggesting
288 that *MAF1*-knockout producer cells should be used when maximal editing efficiencies are
289 required. Additionally, the gene editing efficiencies at a given dose of eVLPs produced
290 from standard cells can in general be achieved using a 2- to 9-fold lower dose of eVLPs
291 produced from *MAF1*-knockout cells (Fig. 4a–i), suggesting that using *MAF1*-knockout
292 cells for eVLP production will be especially beneficial for applications that are constrained
293 by the maximum administrable eVLP dose. Furthermore, by minimizing the eVLP dose
294 required to achieve efficient editing, the use of *MAF1*-knockout producer cells would also
295 reduce the total volume of producer-cell culture required for eVLP production, which could
296 greatly simplify the application of eVLPs in large-scale studies. Importantly, given that
297 several previous studies have identified sgRNA loading into VLPs and related delivery
298 vehicles as a bottleneck that limits delivery potency[8,13,22,37], our discovery that *MAF1*-
299 knockout producer cells improve sgRNA loading into VLPs will likely be widely applicable
300 for RNP delivery using various cell-derived bioparticles.

301 Altogether, our study provides a general workflow for identifying perturbations in
302 producer cells that impact eVLP production and genetically engineering producer cells for
303 improved eVLP production. While previous studies have applied CRISPR screens that
304 use particle-packaged nucleic acid as a way to investigate the cellular determinants of

305 viral vector[38-40] or extracellular vesicle production[41,42], our study is the first to our
306 knowledge that leverages insights from a producer-cell screen to improve VLP production
307 and delivery potency. Notably, our screen design is highly general and can be applied to
308 evaluate various genetic and epigenetic perturbations on a genome-wide scale, including
309 for CRISPR activation or base editing screens. We anticipate that further improvements
310 in particle production are likely possible by employing varied producer-cell perturbations
311 instead of single gene knockouts alone. Overall, while iterative particle architecture
312 engineering continues to improve VLP delivery potency and cell-type targeting
313 capabilities[10,13,22,43], our work establishes producer-cell genetic engineering as a distinct
314 and potentially powerful strategy for maximizing the utility of VLP-based delivery
315 modalities.

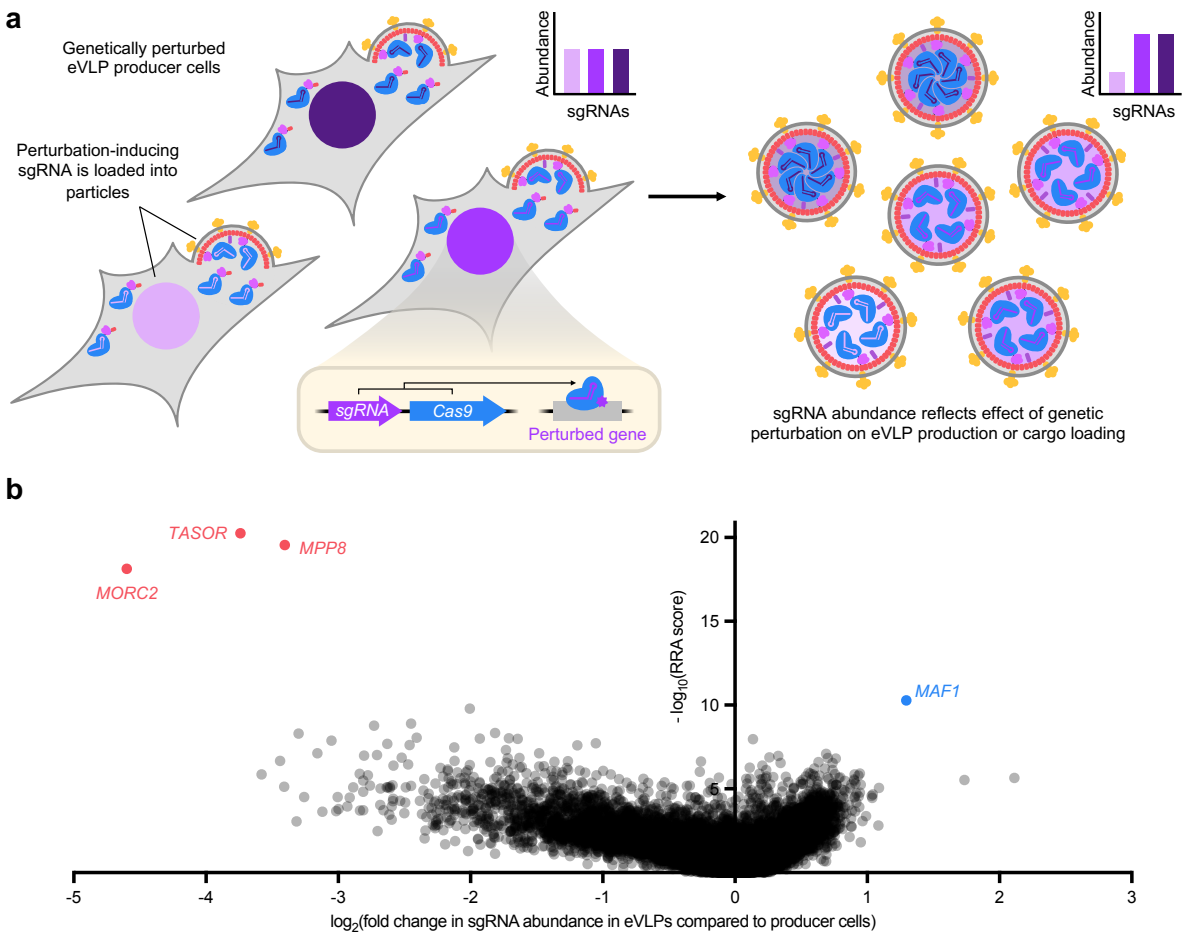

Fig. 1 | Genome-wide screening reveals genetic perturbations that influence eVLP production. a, Overview of the producer-cell screening approach. eVLP production is initiated from a pool of genetically perturbed producer cells, and each eVLP packages sgRNAs that identify the specific genetic perturbation in the cell that produced that particular eVLP. The abundance of a particular sgRNA in eVLPs compared to producer cells reflects how the corresponding genetic perturbation influences eVLP production or cargo loading. **b**, Gene-level phenotypes from the genome-wide knockout screen for cargo-loaded eVLP production. Each gene is represented as a single dot whose x-coordinate reflects the median fold change in sgRNA abundance in eVLPs compared to producer cells for all sgRNAs targeting that particular gene, and whose y-coordinate reflects the MAGeCK RRA score associated with that particular gene (see Methods). Data reflect n=2 screen replicates. See also Extended Data Fig. 1c and Supplementary Table 6.

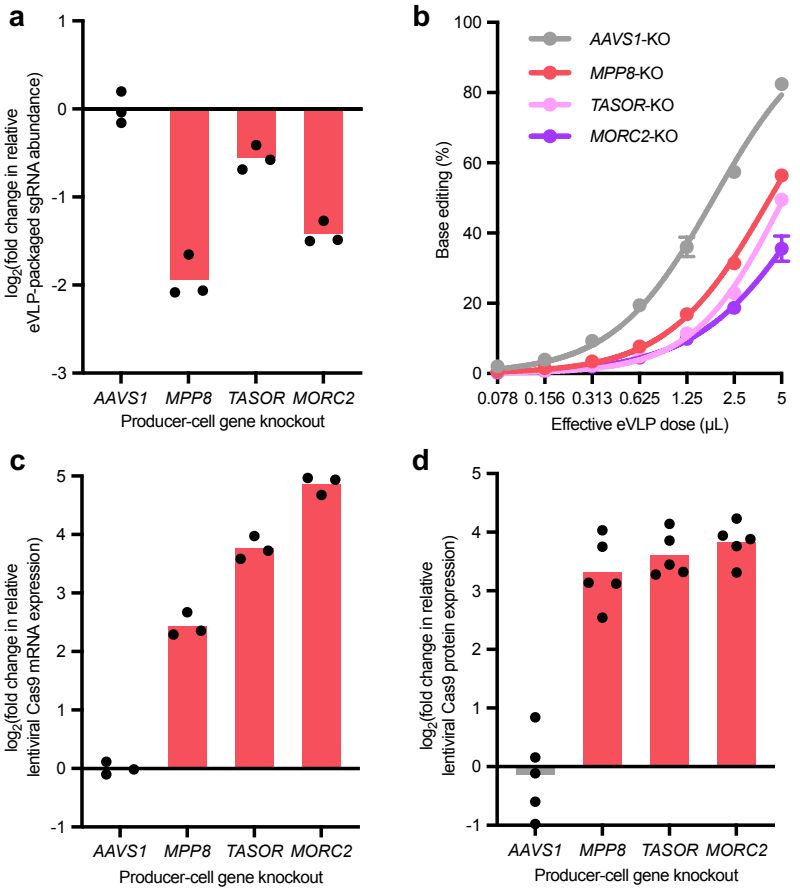

Fig. 2 | Knockout of HUSH-associated genes negatively impacts eVLP sgRNA packaging and delivery potency a, Fold change in eVLP-packaged sgRNA abundance measured by RT-qPCR, normalized relative to sgRNA abundance in eVLPs produced from *AAVS1*-knockout cells. Bars reflect the mean of n=3 replicates, and dots represent individual replicate values. **b**, Comparison of v4 BE-eVLPs produced from *AAVS1*-knockout or HUSH-knockout cells across a range of eVLP doses. Adenine base editing efficiencies at position A_7 of the *BCL11A* +58 enhancer site in HEK293T cells are shown. Dots and error bars represent mean ± s.d. of n=3 biological replicates. Data were fit to four-parameter logistic curves using nonlinear regression. **c**, Fold change in producer-cell Cas9 mRNA abundance measured by RT-qPCR, normalized relative to Cas9 mRNA abundance in *AAVS1*-knockout cells. Bars reflect the mean of n=3 replicates, and dots represent individual replicate values. **d**, Fold change in producer-cell Cas9 protein abundance measured by Western blot, normalized relative to Cas9 protein abundance in *AAVS1*-knockout cells. Bars reflect the mean of n=5 replicates, and dots represent individual replicate values. See also Extended Data Fig. 3a.

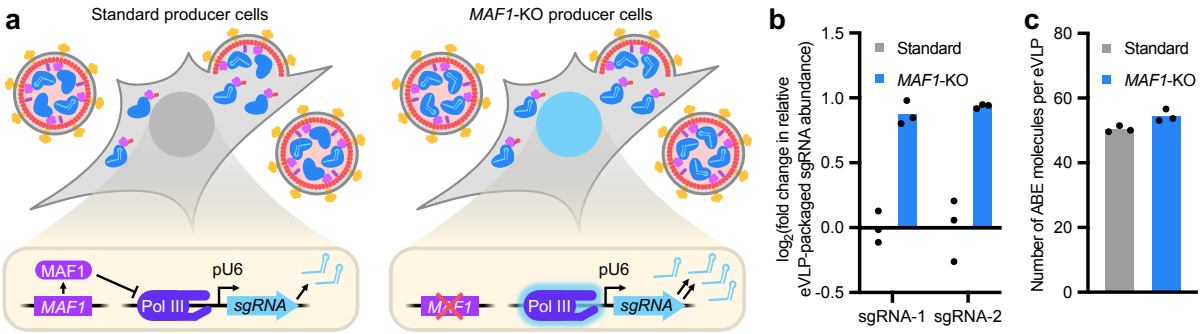

Fig. 3 | *MAF1*-knockout producer cells improve eVLP sgRNA packaging. a, Schematic of standard producer cells versus *MAF1*-knockout producer cells. In standard cells, MAF1 represses RNA Pol III transcription, which limits producer-cell sgRNA expression. In *MAF1*-knockout producer cells, RNA Pol III is no longer subjected to MAF1-mediated repression, which increases sgRNA expression and loading into eVLP-packaged RNPs. **b**, Fold change in eVLP-packaged sgRNA abundance measured by RT-qPCR, normalized relative to sgRNA abundance in eVLPs produced from standard Gesicle cells. sgRNA-1 and sgRNA-2 denote two different packaged sgRNA sequences. **c**, Quantification of ABE molecules per eVLP by anti-Cas9 and anti-MLV p30 ELISA. In **b** and **c**, bars reflect the mean of n=3 replicates, and dots represent individual replicate values.

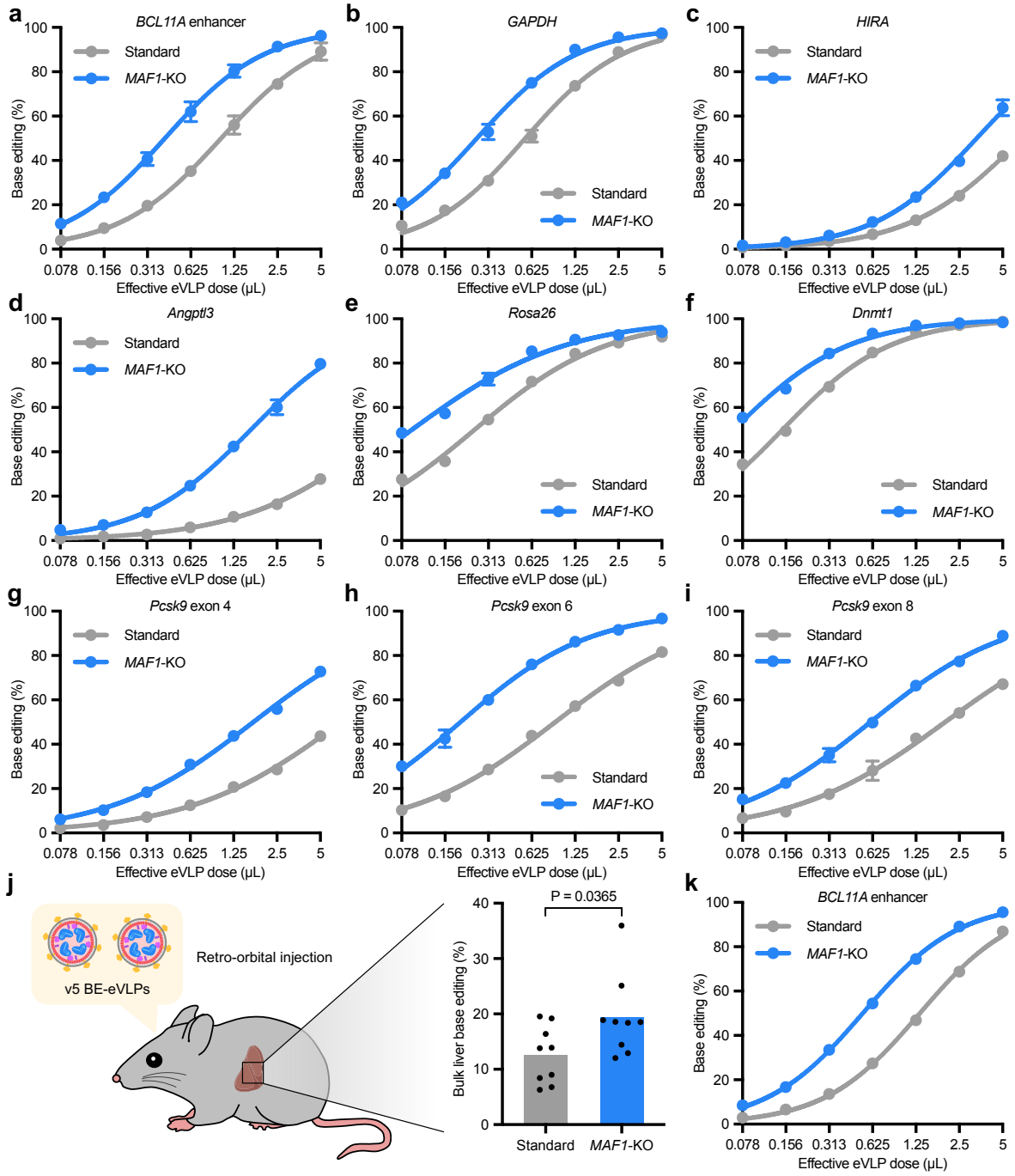

358 **Fig. 4 | *MAF1*-knockout producer cells improve eVLP delivery potency. a–c**,
359 Comparison of v4 BE-eVLPs produced from standard or *MAF1*-knockout Gesicle cells
360 across a range of eVLP doses in HEK293T cells. Adenine base editing efficiencies are
361 shown at position A_7 of the *BCL11A* +58 enhancer site (**a**), position A_7 of the *GAPDH* site
362 (**b**), and position A_5 of the *HIRA* site (**c**). **d–i**, Comparison of v5 BE-eVLPs produced from
363 standard or *MAF1*-knockout Gesicle cells across a range of eVLP doses in mouse Neuro-
364 2a cells. Adenine base editing efficiencies are shown at position A_8 of the *Angptl3* exon 7
365 splice acceptor site (**d**), position A_4 of the *Rosa26* site (**e**), position A_9 of the *Dnmt1* site
366 (**f**), position A_6 of the *Pcsk9* exon 4 splice acceptor site (**g**), position A_4 of the *Pcsk9* exon

6 splice donor site (**h**), and position A_8 of the *Pcsk9* exon 8 splice acceptor site (**i**). **j**, Schematic of mouse experiments and adenine base editing efficiencies at position A_6 of the *Pcsk9* exon 1 splice donor site in bulk mouse liver tissue. Each mouse was injected with 15 µL of 1500-fold concentrated purified eVLPs, corresponding to approximately 3×10^{11} eVLPs (see Methods). Bars reflect the mean of n=9 mice per condition, and dots represent individual mouse values. P-value was calculated using a two-sided unpaired t test. **k**, Comparison of v4 BE-eVLPs produced from standard or *MAF1*-knockout HEK293T/17 cells across a range of eVLP doses in HEK293T cells. Adenine base editing efficiencies at position A_7 of the *BCL11A* +58 enhancer site are shown. In **a–i** and **k**, dots and error bars represent mean ± s.d. of n=4 (**a**) or n=3 (**b–i**, **k**) biological replicates. Data were fit to four-parameter logistic curves using nonlinear regression.

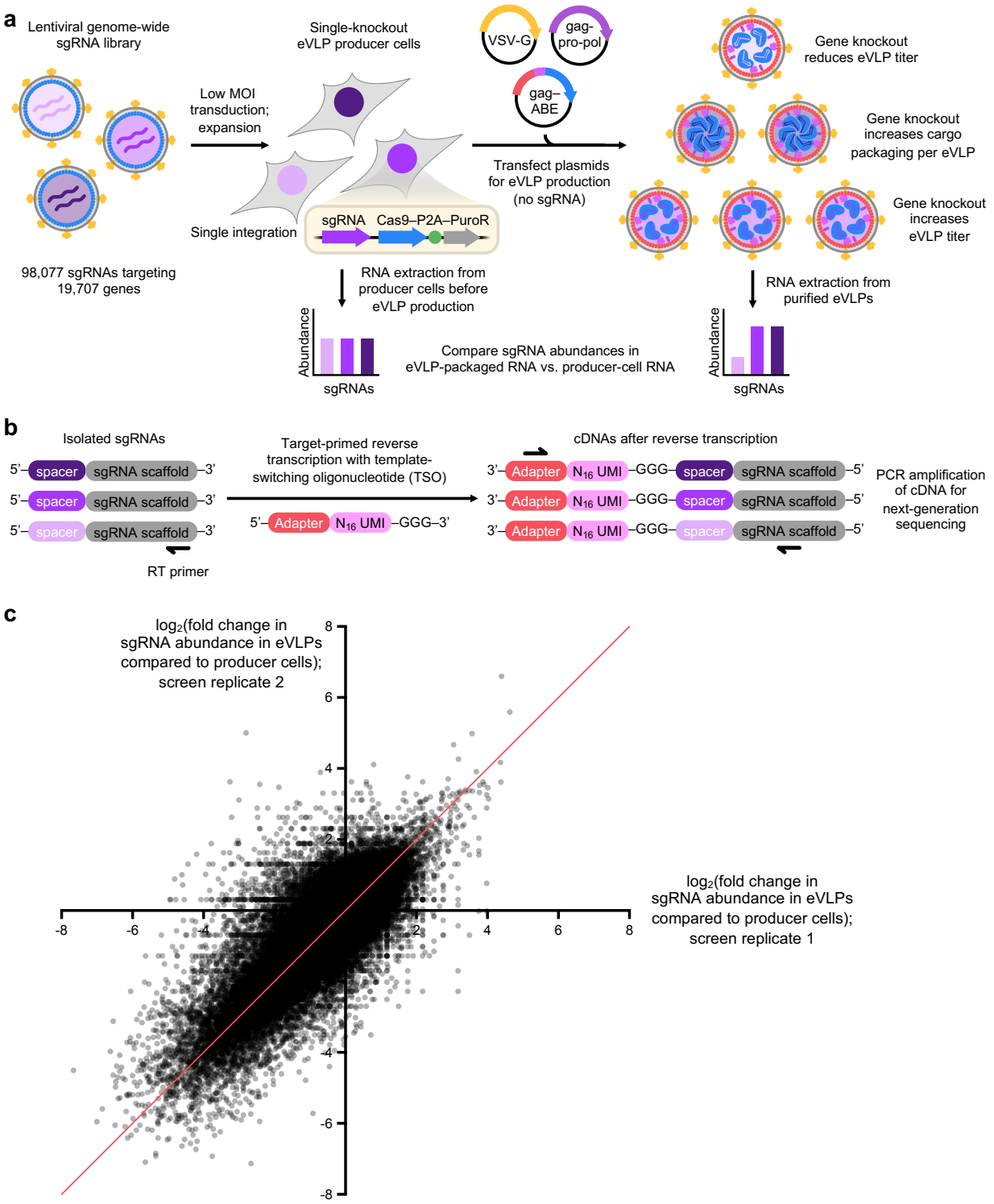

Extended Data Fig. 1 | Genome-wide knockout screening for cargo-loaded eVLP production. a, Overview of the genome-wide knockout screening approach. Low-MOI Cas9/sgRNA lentiviral transduction was used to introduce a genome-wide sgRNA library into Gesicle producer cells, thereby generating a pool of single-knockout producer cells. eVLP production was then initiated from this pool by transfecting expressing eVLP protein

384 components. No additional sgRNA-encoding plasmid was transfected, ensuring that all
385 eVLPs produced from a given producer cell packaged cargo containing the specific
386 knockout-inducing sgRNA that was already introduced into that producer cell by lentiviral
387 transduction. The abundance of a particular sgRNA in eVLPs compared to producer cells
388 reflects how the corresponding gene knockout influences eVLP production or cargo
389 loading. **b**, Schematic of the template-switching reverse transcription approach used for
390 direct-capture sgRNA spacer sequencing from both eVLP-packaged RNA and producer-
391 cell RNA. UMI=unique molecular identifier. **c**, Fold change in sgRNA abundance in eVLPs
392 compared to producer cells across replicates of the genome-wide knockout screen. Each
393 sgRNA in the library is represented as a single dot and reflects the values from n=2 screen
394 replicates. The y=x line is plotted in red. See also Supplementary Tables 3–5.

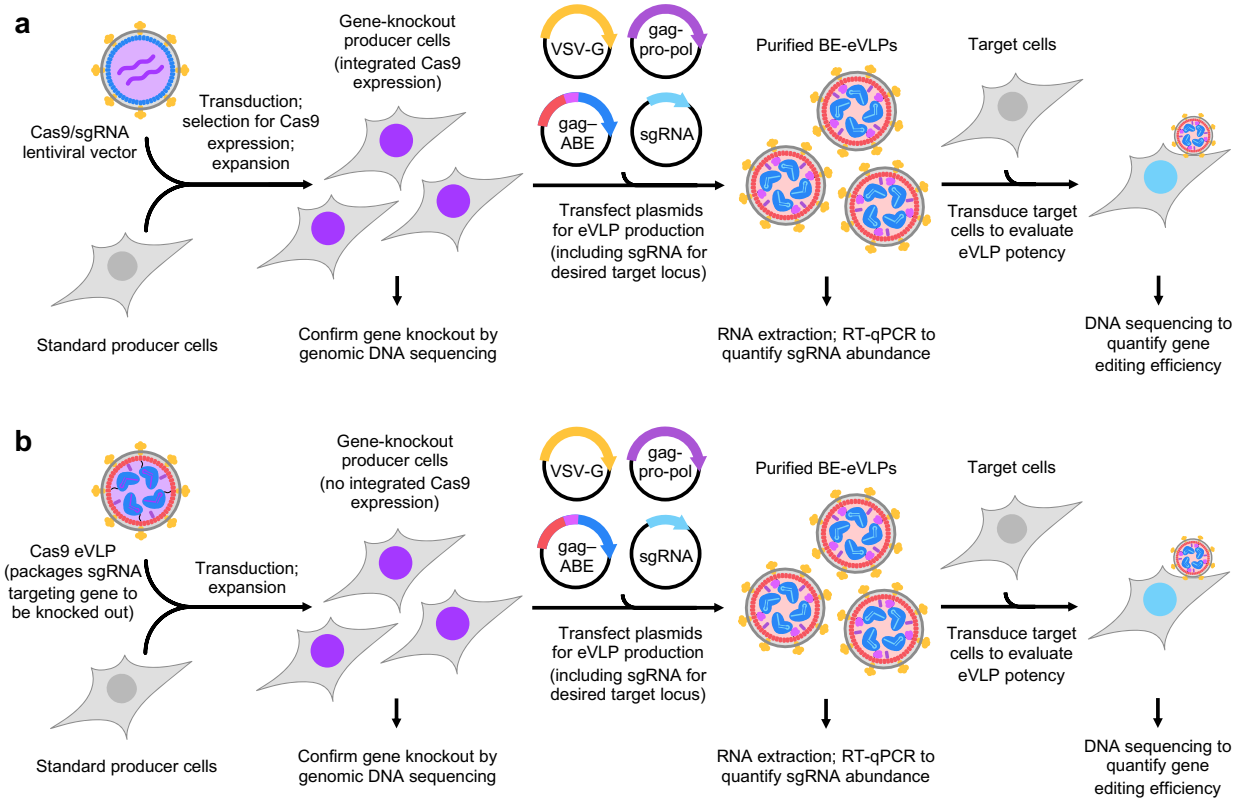

Extended Data Fig. 2 | Generating and characterizing single-knockout producer cell lines. a, Schematic of generating polyclonal single-knockout producer cells via Cas9/sgRNA lentiviral transduction, followed by characterizing the resulting cell lines and their use for eVLP production. **b**, Schematic of generating polyclonal single-knockout producer cells via v4 Cas9-eVLP transduction, followed by characterizing the resulting cell lines and their use for eVLP production.

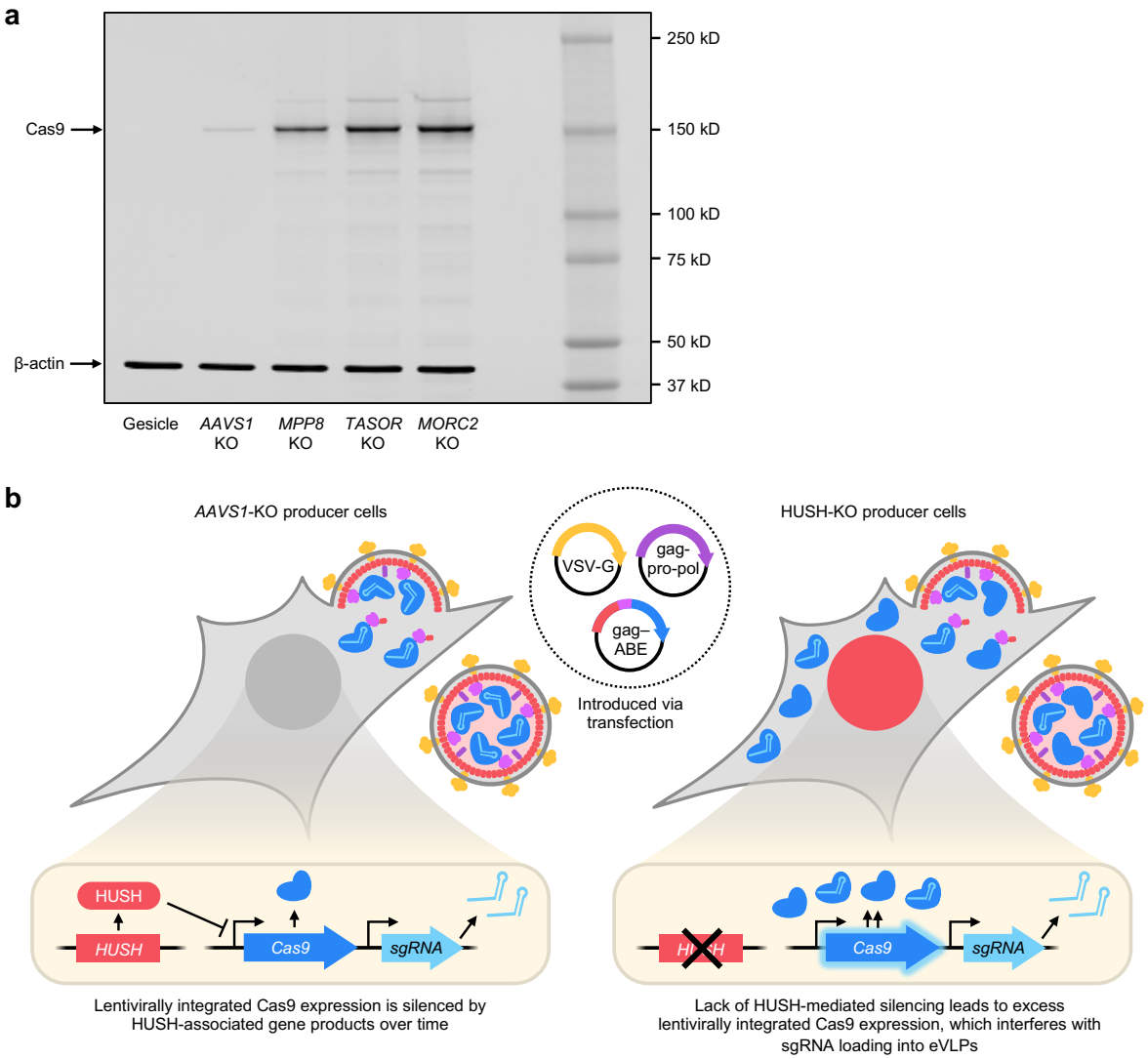

Extended Data Fig. 3 | HUSH-knockout producer cells exhibit increased lentiviral Cas9 expression. a, Western blot analysis of producer-cell protein lysates. **b**, Proposed model for *AAVS1*-knockout producer cells versus HUSH-knockout producer cells. In *AAVS1*-knockout cells, HUSH-associated gene products silence lentivirally integrated Cas9 expression over time. In HUSH-knockout producer cells, lack of HUSH-mediated silencing leads to excess expression of lentivirally integrated Cas9, which interferes with sgRNA loading into eVLPs and therefore reduces eVLP-packaged sgRNA abundance.

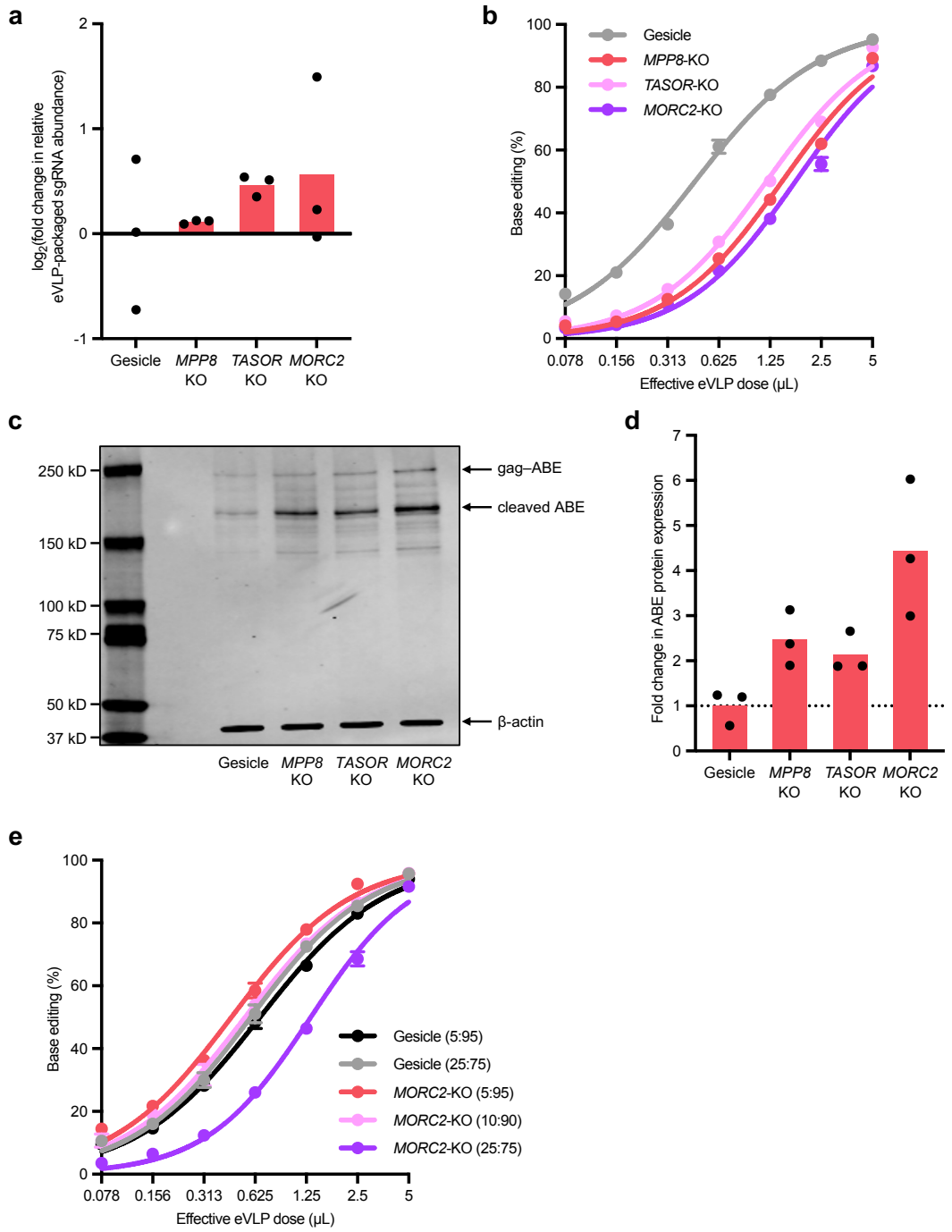

Extended Data Fig. 4 | HUSH-knockout producer cells exhibit increased eVLP cargo expression. a, Fold change in eVLP-packaged sgRNA abundance measured by RT-qPCR, normalized relative to sgRNA abundance in eVLPs produced from Gesicle cells. Bars reflect the mean of n=3 replicates, and dots represent individual replicate values. **b**, Comparison of v4 BE-eVLPs produced from Gesicle or HUSH-knockout cells across a range of eVLP doses. Adenine base editing efficiencies at position A_7 of the *BCL11A* +58 enhancer site in HEK293T cells are shown. Dots and error bars represent mean ± s.d. of n=3 biological replicates. Data were fit to four-parameter logistic curves using nonlinear

419 regression. **c**, Western blot analysis of protein lysates from producer cells transfected
420 with eVLP production plasmids. The full-length gag–ABE fusion is ~247 kD and the
421 cleaved ABE (following viral protease-mediated cleavage) is ~184 kD. **d**, Fold change in
422 transfected-producer-cell ABE protein abundance measured by Western blot, normalized
423 relative to ABE protein abundance in transfected Gesicle cells. Bars reflect the mean of
424 n=3 replicates, and dots represent individual replicate values. **e**, Comparison of v4 BE-
425 eVLPs produced from Gesicle or *MORC2*-knockout cells across a range of eVLP doses
426 using different transfected eVLP plasmid stoichiometries. Values in parentheses reflect
427 the gag–ABE:gag–pro–pol plasmid ratio used for eVLP production. Adenine base editing
428 efficiencies at position A_7 of the *BCL11A* +58 enhancer site in HEK293T cells are shown.
429 Dots and error bars represent mean ± s.d. of n=3 biological replicates. Data were fit to
430 four-parameter logistic curves using nonlinear regression.

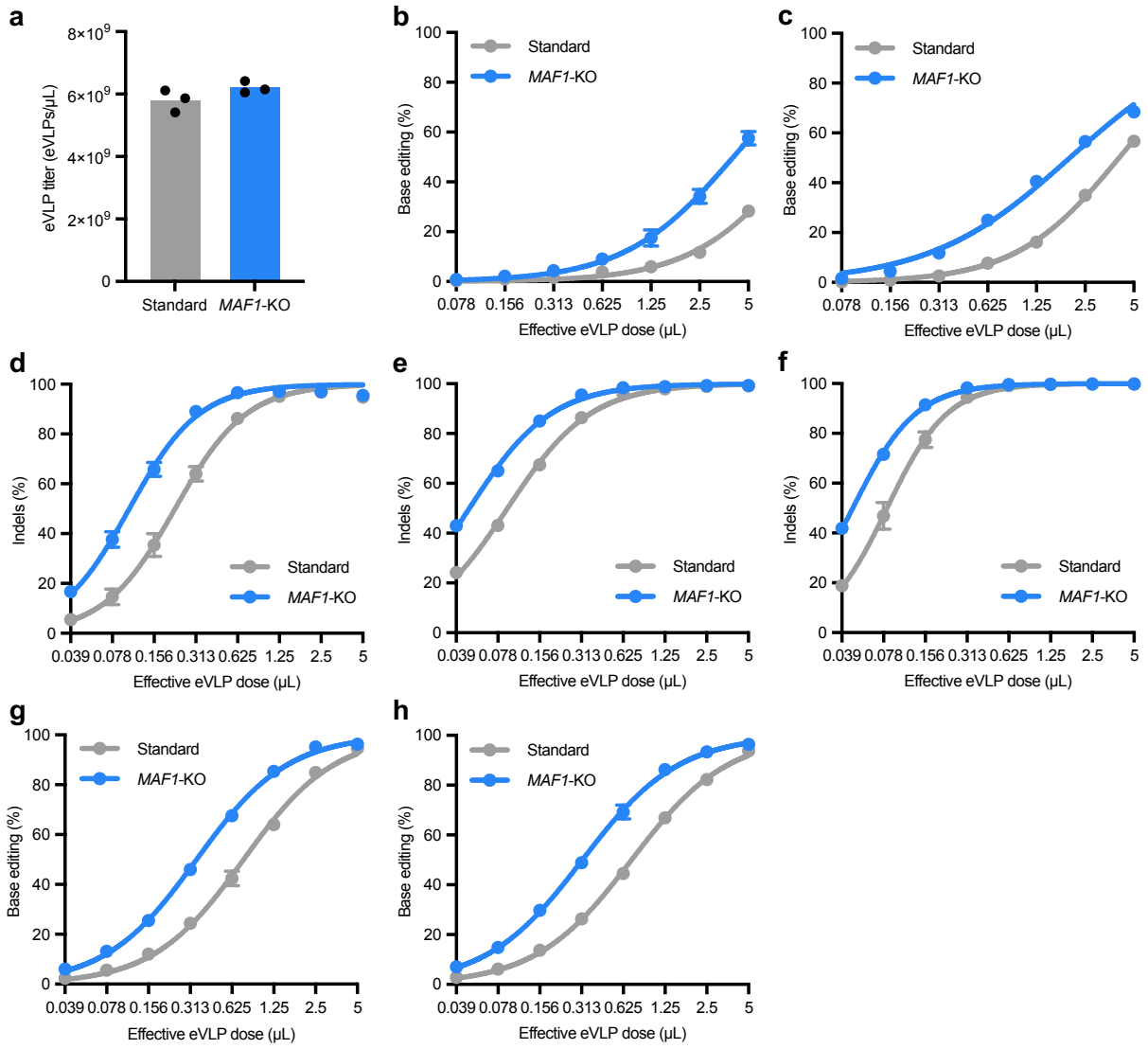

Extended Data Fig. 5 | *MAF1*-knockout producer cells improve eVLP delivery potency. a, Quantification of eVLP titer by anti-MLV p30 ELISA (see Methods). Bars reflect the mean of n=3 replicates, and dots represent individual replicate values. **b**, Comparison of v4 ABE8e-NG-eVLPs produced from standard or *MAF1*-knockout Gesicle cells across a range of eVLP doses. Adenine base editing efficiencies at position A_7 of the *BCL11A* +58 enhancer site in HEK293T cells are shown. **c**, Comparison of v4 TadCBEa-eVLPs produced from standard or *MAF1*-knockout Gesicle cells across a range of eVLP doses. Cytosine base editing efficiencies at position C_6 of the *BCL11A* +58 enhancer site in HEK293T cells are shown. **d–f**, Comparison of v4 Cas9-eVLPs produced from standard or *MAF1*-knockout Gesicle cells across a range of eVLP doses in HEK293T cells. Indel frequencies are shown at the *BCL11A* +58 enhancer site (**d**), *HEK2* site (**e**), and *EMX1* site (**f**). **g–h**, Comparison of ABE8e-packaging ENVLPE$^+$ particles (**g**) or v4 ABE8e-eVLPs (**h**) produced from standard or *MAF1*-knockout Gesicle cells across a range of doses. Adenine base editing efficiencies at position A_7 of the *BCL11A* +58 enhancer site in HEK293T cells are shown. **b–h**, Dots and error bars represent mean ±

447 s.d. of n=3 biological replicates. Data were fit to four-parameter logistic curves using
448 nonlinear regression.
449

Methods

Cloning

Plasmids used in this study were cloned via Gibson cloning (NEBuilder® HiFi DNA Assembly; E2621X) or Golden Gate cloning. DNA was amplified via PCR using Phusion HotStart II polymerase (Thermo Fisher Scientific; F537L). Mach1 (Thermo Fisher Scientific; C862003) or NEB® Stable (New England Biolabs; C3040H) chemically competent *E. coli* were used for plasmid propagation. Plasmids were isolated using QIAGEN Plasmid Plus Midi (12945) or Maxi (12963) Kits according to the manufacturer's protocols.

Cell culture

HEK293T cells (ATCC; CRL-3216), Gesicle Producer 293T cells (Takara; 632617), HEK293T/17 cells (ATCC; CRL-11268), and Neuro-2a cells (ATCC; CCL-131) were maintained in DMEM + GlutaMAX (Life Technologies; 10569044) supplemented with 10% (v/v) fetal bovine serum (Gibco; A5670701). Cells were cultured at 37 °C with 5% carbon dioxide and were confirmed to be negative for mycoplasma by testing with MycoAlert (Lonza; LT07-318).

eVLP production and purification

eVLPs were produced as described previously[8,22]. Briefly, eVLPs were produced by transient transfection of Gesicle 293T cells, HEK293T/17 cells, or variants thereof as noted in the main text and figure legends. Producer cells were seeded in T-75 flasks at a density of 5×10^6 cells per flask. After 20–24 h, cells were transfected using the jetPRIME transfection reagent (Polyplus; 114-75) according to the manufacturer's protocols. For producing eVLPs, a mixture of plasmids expressing VSV-G (400 ng), MMLV gag-pro-pol (3,375 ng), gag–cargo (1,125 ng), and an sgRNA (4,400 ng) was co-transfected per T-75 flask.

40–48 h post-transfection, producer cell supernatant was harvested and centrifuged for 5 min at 500 g to remove cell debris. The clarified eVLP-containing supernatant was filtered through a 0.45-µm PVDF filter (Millipore; SE1M003M00). The filtered supernatant was concentrated 100-fold using PEG-it Virus Precipitation Solution (System Biosciences; LV825A-1) according to the manufacturer's protocols and resuspended in Opti-MEM serum-free media (Thermo Fisher Scientific; 31985070). For eVLPs prepared for protein or RNA quantification, or those that were injected into mice, the filtered supernatant was concentrated 1500-fold by ultracentrifugation using a cushion of 20% (w/v) sucrose in PBS. Ultracentrifugation was performed at 26,500 rpm (86,242 g) for 2 h (4ºC) using an SW32 Ti rotor in an Optima XE Ultracentrifuge (Beckman Coulter). Following ultracentrifugation, eVLP pellets were resuspended in cold PBS pH 7.4 (Gibco; 10010023) and centrifuged at 1,000 g for 5 min to remove debris. eVLPs were frozen at a rate of -1ºC/min and stored at -80ºC. eVLPs were thawed on ice immediately prior to use.

eVLP transduction and genomic DNA isolation

Cells were transduced with eVLPs as described previously[8,22] with a few modifications. Cells were plated for transduction in 96-well plates at a density of 16,000 cells per well.

After 20–24 h, eVLPs were added directly to the culture media in each well. In general, eVLPs were serially diluted by 2-fold to generate dose titration curves, and a constant volume of 5 µL of eVLP-containing solution was added to each well. 48–72 h post-transduction, cellular genomic DNA was isolated. Media was aspirated from each well, and 60 µL of lysis buffer (10 mM Tris-HCl pH 8.0, 0.05% SDS, 25 µg mL^{-1} Proteinase K (Thermo Fisher Scientific; EO0492)) was added to each well. Lysis was achieved by incubation at 37 ºC for 1–1.5 h followed by heat inactivation at 80ºC for 30 min.

High-throughput sequencing of genomic DNA

Genomic DNA was isolated as described above. Following genomic DNA isolation, 1 µL of the isolated DNA (1–10 ng) was used as input for the first of two PCR reactions. Genomic loci were amplified in PCR1 using Phusion U polymerase (Thermo Fisher Scientific; F562L). PCR1 primers are listed in Supplementary Table 2 under the HTS_forward and HTS_reverse columns. PCR1 was performed as follows: 95 ºC for 3 min; 30 cycles of 95 ºC for 15 s, 61 ºC for 20 s, and 72 ºC for 30s; 72ºC for 1 min. PCR1 products were confirmed on a 1% agarose gel. 1 µL of PCR1 was used as an input for PCR2 to install Illumina barcodes. PCR2 was conducted for nine cycles of amplification using Phusion HotStart II polymerase (Thermo Fisher Scientific; F537L). Following PCR2, samples were pooled and gel purified in a 1% agarose gel using a QIAquick Gel Extraction Kit (Qiagen; 28704). Library concentration was quantified using the Qubit High-Sensitivity Assay Kit (Thermo Fisher Scientific; Q33230). Samples were sequenced on an Illumina MiSeq instrument (paired-end read, read 1: 200–280 cycles, read 2: 0 cycles) using an Illumina MiSeq 300 v2 Kit (Illumina).

High-throughput sequencing data analysis for base editing experiments

Sequencing reads were demultiplexed using the MiSeq Reporter software (v2.6) (Illumina) and were analyzed using CRISPResso2 (ref. [44]) (v2.3.2) as previously described[8]. Batch analysis mode (one batch for each unique amplicon and sgRNA combination analyzed) was used in all cases. Reads were filtered by minimum average quality score (Q > 30) prior to analysis. The following quantification window parameters were used: -w 20 -wc -10. Base editing efficiencies are reported as the percentage of sequencing reads containing a given base conversion at a specific position. Prism 10 (GraphPad) was used to generate dot plots and bar plots.

Lentiviral vector production

Lentiviral vectors were constructed via Golden Gate cloning into the LentiCRISPRv2-Opti backbone, a gift from the Whitehead Institute Functional Genomics Platform (Addgene #163126). Plasmids were propagated in NEB® Stable (New England Biolabs; C3040H) chemically competent *E. coli*. Prior to lentiviral vector production, HEK293T/17 cells were maintained in antibiotic-free DMEM supplemented with 10% fetal bovine serum (v/v). On day 1, 5×10^6 cells were plated in 10 mL of media in T-75 flasks. The following day, cells were transfected with 6 µg of VSV-G envelope plasmid, 9 µg of psPAX2 (plasmid encoding viral packaging proteins) and 9 µg of transfer vector plasmid diluted in 1,500 µL Opti-MEM with 70 µL of FuGENE HD transfection reagent (Promega; E2312). Two days after transfection, media was centrifuged at 500 *g* for 5 min to remove cell debris followed by filtration using a 0.45-µm PVDF vacuum filter (Millipore; SE1M003M00). The filtered

542 supernatant was concentrated using PEG-it Virus Precipitation Solution (System
543 Biosciences; LV825A-1) according to the manufacturer's protocols and resuspended in
544 Opti-MEM serum-free media (Gibco; 31985070).
545
546 **sgRNA library propagation**
547 For the genome-wide knockout screen, a previously described human genome-wide
548 sgRNA library containing 98,077 unique sgRNAs targeting 19,707 genes across the
549 human genome[24] was obtained as a gift from the Whitehead Institute Functional
550 Genomics Platform. sgRNA sequences are listed in Supplementary Table 3. Vectors
551 contained pU6-sgRNA expression cassettes along with pEFS-Cas9-P2A-PuroR
552 (LentiCRISPRv2-Opti backbone, Addgene #163126). The plasmid library was
553 propagated as follows. First, electrocompetent cells were generated from NEB® Stable
554 (New England Biolabs; C3040H) chemically competent *E. coli* by growing single colonies
555 to mid-log phase in LB media containing 10 µg/mL tetracycline and 50 µg/mL
556 streptomycin, collecting cells by centrifugation at 5,000 g for 1 min at 4 ºC, washing with
557 cold 10% (v/v) glycerol, and repeating for a total of four washes. Freshly prepared
558 electrocompetent cells were transferred to a chilled 0.1 cm electroporation cuvette (Bio-
559 Rad; 1652089) and mixed with the purified, assembled library plasmids. Cells were
560 electroporated using a time-constant protocol with t = 5 ms at 1.5 kV. Electroporated cells
561 were recovered at 37 ºC for 25 min with shaking. Recovered cells were plated onto 500
562 cm^2 plates containing LB media + 1.5% agar supplemented with 100 µg/mL carbenicillin
563 and incubated for 16 h at 37 ºC. After overnight incubation, colonies were scraped into
564 LB media and cells were collected by centrifugation. Plasmids were purified using a
565 Plasmid Plus Maxi Kit (Qiagen; 12963) according to the manufacturer's protocols. sgRNA
566 representation in the propagated plasmid library was confirmed via targeted amplicon
567 sequencing.
568
569 **Genome-wide knockout screen for cargo-loaded eVLP production**
570 Lentiviral libraries were produced as described above and were concentrated ~66-fold by
571 PEG precipitation. Gesicle cells were seeded at a density of 1.5×10^7 cells per T-175 and
572 immediately transduced with 105 µL of concentrated lentivirus. A total of 2.4×10^8 Gesicle
573 cells were seeded for transduction. 24 h after transduction, cells were trypsinized and
574 reseeded at half the original density in media supplemented with 2 µg/mL puromycin.
575 Puromycin selection was continued for 7 days, during which time cell viability was
576 monitored and cells were expanded upon reaching confluency. The initial multiplicity of
577 infection (MOI) was inferred by counting surviving cells and assuming a doubling time of
578 24 h. Using this method, the MOI was calculated to be 0.28, corresponding to
579 approximately 660x coverage of the sgRNA library. A minimum of 1×10^8 cells were carried
580 forward each time the cells were passaged to retain overall coverage.
581 After cells were robustly surviving puromycin selection (~1 week), cells were
582 seeded for eVLP production in T-75 flasks at a density of 5×10^6 cells/flask. At this time,
583 1×10^8 cells were collected by centrifugation, and the cell pellet was frozen at -80ºC and
584 reserved for RNA extraction (see below). 24 h after seeding, cells were transfected using
585 the jetPRIME transfection reagent (Polyplus; 114-75) according to the manufacturer's
586 protocols. A mixture of pUC19 (4,400 ng), VSV-G (400 ng), MMLV gag-pro-pol (3,375 ng),
587 and MMLVgag–ABE8e (1,125) plasmids were co-transfected per T-75 flask. 42 h post

transfection, eVLPs were harvested and filtered as described above. The filtered supernatant was concentrated by sucrose-cushion ultracentrifugation as described above. Following ultracentrifugation, eVLP pellets were resuspended in cold PBS pH 7.4 (Gibco; 10010023). Purified eVLPs were treated with DNase (Qiagen; 79254) followed by RNA extraction using the QIAmp Viral RNA Mini Kit (Qiagen; 52904) according to the manufacturer's protocols. RNA was extracted from the producer-cell pellet using QIAzol Lysis Reagent (Qiagen; 79306) according to the manufacturer's protocols. This entire process of seeding single-knockout Gesicle cells followed by eVLP production and RNA extractions was performed twice on different days for two screen replicates.

Following RNA extraction, both producer-cell and eVLP RNA were reverse transcribed using the Maxima Reverse Transcriptase (Thermo Fisher Scientific; EP0742) according to the manufacturer's protocols. Primers and other oligonucleotides used for target-primed sgRNA reverse transcription are listed in Supplementary Table 1. The RT primer was added at a final concentration of 1 μM in the RT reaction. Following incubation at 50ºC for 20 min, the template-switching oligo (TSO) was spiked in to the reaction at a final concentration of 1 μM. The reaction was incubated for a further 20 min at 50ºC, and heat inactivated at 85ºC for 5 min. For producer-cell RNA only, the RT products were further processed by hydrolyzing the RNA in 0.2 M NaOH (final concentration) and heating at 90ºC for 10 min, cleaning up with the MinElute Reaction Cleanup Kit (Qiagen; 28104) according to the manufacturer's protocols, and left size selection using SPRIselect (Beckman Coulter; B23317) at a 1.5x bead ratio to remove smaller products and residual primers. Producer-cell cDNAs were subsequently amplified for sequencing with the KAPA HiFi HotStart ReadyMix (Roche Diagnostics; 09420398001) using 2.5 μL of cDNA input per 25 μL reaction and the following conditions: 95 ºC for 3 min; 20 cycles of 98 ºC for 20 s, 61 ºC for 20 s, and 72 ºC for 30s; 72ºC for 2 min. eVLP cDNAs were amplified for sequencing with the KAPA HiFi HotStart ReadyMix using 2.5 μL of cDNA input per 25 μL reaction and the following conditions: 95 ºC for 3 min; 14 cycles of 98 ºC for 20 s, 61 ºC for 20 s, and 72 ºC for 30s; 72ºC for 2 min. Illumina barcodes were installed using KAPA HiFi HotStart ReadyMix using 2 μL of PCR1 input per 25 μL reaction and the following conditions: 95 ºC for 3 min; 9 cycles of 98 ºC for 20 s, 61 ºC for 20 s, and 72 ºC for 30s; 72ºC for 2 min. Following PCR2, samples were gel purified in a 1% agarose gel using a QIAquick Gel Extraction Kit (Qiagen; 28704). Library concentration was quantified using the Qubit High-Sensitivity Assay Kit (Thermo Fisher Scientific; Q33230). Samples were sequenced on an Illumina NextSeq instrument (paired-end read, read 1: 76 cycles, read 2: 0 cycles) using an Illumina NextSeq 75-cycle High-Output v2.5 Kit (Illumina).

Genome-wide knockout screen analysis

Code used for processing sequencing reads from the genome-wide knockout screen is provided in Supplementary Note 1. Briefly, sequencing reads were demultiplexed using bcl2fastq (v2.20.0.422). Reads were trimmed using seqkit[45] (v2.6.1) to restrict analysis to the UMI and sgRNA protospacer sequences only. Then, reads were UMI-deduplicated using AmpUMI[46] and trimmed with seqkit to remove the UMI and restrict subsequent analysis to the sgRNA protospacer sequences only. Processed reads were aligned to a reference fasta file containing all sgRNA sequences using bowtie[47] (v1.3.1), and sgRNA counts were generated from alignments as previously described[24]. Raw sgRNA counts are provided in Supplementary Table 4. MAGeCK[48] (v0.5.9.5) was used to quantify gene-

level phenotypes from the sgRNA counts. Producer-cell samples were treated as "control" samples and eVLP samples were treated as "treatment" samples for the purpose of MAGeCK analysis. Median-normalized sgRNA read counts and fold changes are provided in Supplementary Table 5, and gene-level phenotypes are provided in Supplementary Table 6. For genes with a positive median $\log_2$ fold change, the positive MAGeCK RRA score, p-value, and FDR were used, and for genes with a negative median $\log_2$ fold change, the negative MAGeCK RRA score, p-value, and FDR were used. Prism 10 (GraphPad) was used to generate dot plots.

Generation of knockout cell lines

To generate knockout cell lines via Cas9/sgRNA lentiviral transduction, lentiviral vectors were cloned and produced as described above. Cells were seeded in T-75 flasks at a density of 5×10^6 cells/flask and immediately transduced with 50 µL of concentrated lentivirus. 24 h after transduction, cells were trypsinized and reseeded in media supplemented with 2 µg/mL puromycin. Puromycin selection was continued, during which time cell viability was monitored and cells were expanded upon reaching confluency. After cells were robustly surviving puromycin selection (~1 week), cells were harvested and genotyped via targeted-amplicon high-throughput sequencing as described above to confirm gene knockout. Cell lines were regularly genotyped over time to confirm continued gene knockout.

To generate knockout cell lines via Cas9-eVLP transduction, v4 Cas9-eVLPs were produced as described above. Cells were seeded in 96-well plates at a density of 16,000 cells per well. 24 h after seeding, cells were transduced with 5 µL of purified Cas9-eVLPs per well. 72 h after eVLP transduction, cells were harvested and genotyped via targeted-amplicon high-throughput sequencing as described above to confirm gene knockout. Cells were expanded and regularly genotyped over time to confirm continued gene knockout.

eVLP-packaged sgRNA extraction and RT-qPCR

eVLPs for RNA extraction were purified via sucrose-cushion ultracentrifugation as described above. Purified eVLPs were treated with DNase (Qiagen; 79254) followed by RNA extraction using the QIAmp Viral RNA Mini Kit (Qiagen; 52904) according to the manufacturer's protocols. Extracted RNA was reverse transcribed using SuperScript™ III First-Strand Synthesis SuperMix (Thermo Fisher Scientific; 18080400) and an sgRNA-specific DNA primer (see Supplementary Table 1) according to the manufacturer's protocols. qPCR analysis of the resulting cDNA was performed using a QuantStudio™ 3 Real-Time PCR System (Thermo Fisher Scientific) with SYBR green dye (Lonza; 50512). The relative eVLP-packaged sgRNA abundance was calculated as $\log_2$[fold change] (ΔC_t) relative to control eVLPs (i.e. those produced from standard or *AAVS1*-knockout cells).

Producer-cell RNA extraction and RT-qPCR

Cellular RNA was extracted using the RNeasy Plus Mini Kit (Qiagen; 74136) according to the manufacturer's protocols. Extracted RNA was reverse transcribed using SuperScript™ III First-Strand Synthesis SuperMix (Thermo Fisher Scientific; 18080400) using random hexamer primers according to the manufacturer's protocols. qPCR analysis of the resulting cDNA was performed using a QuantStudio™ 3 Real-Time PCR System

680 (Thermo Fisher Scientific) with SYBR green dye (Lonza; 50512). The relative Cas9
681 mRNA abundance across different producer cells was calculated via the $\Delta\Delta C_t$ method
682 using *ACTB* as the housekeeping gene. qPCR primers are listed in Supplementary Table
683 1.
684
685 **Producer-cell protein extraction and Western blot analyses**
686 For producer-cell protein extraction, 1×10^6 cells were collected by centrifugation at 500 g
687 for 5 min. Cell pellets were washed once with 1 mL of cold PBS and lysed using RIPA
688 buffer (Thermo Fisher Scientific; 89901) supplemented with cOmplete™ protease
689 inhibitor cocktail (Roche Diagnostics; 11836153001) according to the manufacturer's
690 protocols. Cells were lysed at 4ºC for 30 min with gentle agitation. The lysate was clarified
691 by centrifugation at 10,000 g for 20 min at 4ºC, and the clarified supernatant was
692 combined with 4x Laemmli Sample Buffer (Bio-Rad; 1610747) and heated at 95ºC for 10
693 min. Protein extracts were subsequently separated by electrophoresis at 150 V for 45 min
694 on a NuPAGE 3–8% Tris-Acetate gel (Thermo Fisher Scientific; EA0378BOX) in 1x
695 NuPAGE Tris-Acetate SDS running buffer (Thermo Fisher Scientific; LA0041). Transfer
696 to a PVDF membrane was performed using an iBlot 2 Gel Transfer Device (Thermo Fisher
697 Scientific) at 20 V for 7 min. The membrane was blocked for 1 h at room temperature with
698 rocking in blocking buffer: 1% bovine serum albumin (BSA) and 0.1% Tween-20 in TBS
699 (150 mM NaCl and 50 mM Tris-HCl). After blocking, the membrane was incubated
700 overnight at 4ºC with rocking with mouse anti-Cas9 (Cell Signaling Technology; 14697,
701 1:1000 dilution) and rabbit anti-actin (Cell Signaling Technology; 4970, 1:1000 dilution).
702 The membrane was washed three times with 1xTBST (150 mM NaCl, 0.5% Tween-20,
703 and 50 mM Tris-HCl) for 10 min each time at room temperature, then incubated with goat
704 anti-mouse secondary antibody (LI-COR IRDye 680RD; 926-68070, 1:10000 dilution in
705 blocking buffer) and goat anti-rabbit secondary antibody (LI-COR IRDye 800CW; 926-
706 32211, 1:10000 dilution in blocking buffer) for 1 h at room temperature with rocking. The
707 membrane was washed as before and imaged using an Odyssey Imaging System (LI-
708 COR). Protein abundances were quantified by densitometry using ImageJ (v2.14.0).
709 Cas9 abundances were normalized to the actin abundance within each sample, and
710 comparisons across samples were performed using these actin-normalized values.
711 For protein extraction from cells transfected with eVLP production plasmids, cells
712 were first seeded for eVLP production in T-75 flasks as described above. 24 h after
713 seeding, cells were transfected with all eVLP production plasmids except the VSV-G
714 plasmid. 48 h after transfection, cells were trypsinized and collected by centrifugation,
715 and were then processed as described above.
716
717 **eVLP protein content quantification**
718 eVLP protein content quantification was performed as described previously[8]. Briefly,
719 ultracentrifuge-purified eVLPs were lysed in dye-free Laemmli sample buffer (50 mM Tris-
720 HCl pH 7.0, 2% sodium dodecyl sulfate (SDS), 10% (v/v) glycerol, 2 mM dithiothreitol
721 (DTT)) by heating at 95ºC for 15 min. The concentration of ABE protein in purified eVLPs
722 was quantified using the FastScan™ Cas9 (*S. pyogenes*) ELISA kit (Cell Signaling
723 Technology; 29666C) according to the manufacturer's protocols. Recombinant Cas9 (*S.*
724 *pyogenes*) nuclease protein (New England Biolabs; M0386) was used to generate the
725 standard curve for quantification. The concentration of MLV p30 protein in purified eVLPs

726 was quantified using the MuLV Core Antigen ELISA kit (Cell Biolabs; VPK-156) according
727 to the manufacturer's protocols. The number of ABE protein molecules per eVLP was
728 calculated by determining the ratio of Cas9 molecules to p30 molecules and assuming a
729 copy number of 1800 molecules of p30 per eVLP as previously described[8].
730
731 **Animal experiments**
732 All mouse experiments were compliant with relevant ethical regulations and were
733 approved by the MIT Committee on Animal Care (D16-00078; 2402000629). Wild-type 8-
734 week-old adult male C57BL/6J mice (000664) were purchased from the Jackson
735 Laboratory. All mice were housed in a room maintained on a 12 h light and dark cycle
736 with *ad libitum* access to standard rodent diet and water. Animals were randomly
737 assigned to various experimental groups.
738 Retro-orbital injections were performed as described previously[8] with a few
739 modifications. eVLPs for retro-orbital injections were purified via sucrose-cushion
740 ultracentrifugation as described above. Immediately prior to injection, eVLPs were
741 partially clarified by centrifugation at 1000 g for 5 min to remove debris. The eVLP-
742 containing supernatant was diluted with 0.9% NaCl (Hospira; 00409-4888-10), and a total
743 of 100 μL solution (containing 15 μL of 1500-fold concentrated purified eVLPs,
744 approximately 3×10^{11} eVLPs) was injected per mouse. Genomic DNA was purified from
745 bulk liver tissue using the Agencourt DNAdvance kit (Beckman Coulter; A48705)
746 according to the manufacturer's protocols. Purified genomic DNA was amplified for high-
747 throughput sequencing as described above, with 25 cycles of amplification during PCR1.
748
749 **ENVLPE$^+$ production**
750 ENVLPE$^+$ particles[10] were produced analogously to eVLPs. Producer cells were seeded
751 in T-75 flasks at a density of 5×10^6 cells per flask. After 20–24 h, cells were transfected
752 using the jetPRIME transfection reagent (Polyplus; 114-75) according to the
753 manufacturer's protocols. A mixture of plasmids expressing VSV-G (1550 ng), psPAX2-
754 D64V (1,149 ng; Addgene #63586, a gift from David Rawlings & Andrew Scharenberg),
755 pCMV_ENVLPE+ (665 ng; Addgene #232427, a gift from Gil Westmeyer),
756 pCMV_ABE8e_superNLS (1,023 ng; Addgene #232429, a gift from Gil Westmeyer), and
757 a *BCL11A*-targeting PP7-containing sgRNA (4,913 ng; cloned from Addgene #232432, a
758 gift from Gil Westmeyer) were co-transfected per T-75 flask. 40–48 h post-transfection,
759 producer cell supernatant was harvested and centrifuged for 5 min at 500 g to remove
760 cell debris. The clarified ENVLPE$^+$-containing supernatant was filtered through a 0.45-μm
761 PVDF filter (Millipore; SE1M003M00). The filtered supernatant was concentrated 100-fold
762 using PEG-it Virus Precipitation Solution (System Biosciences; LV825A-1) according to
763 the manufacturer's protocols and resuspended in Opti-MEM serum-free media (Thermo
764 Fisher Scientific; 31985070).
765
766 **Statistical analysis**
767 Data are presented as mean and standard deviation (s.d.). No statistical methods were
768 used to predetermine sample size. Statistical analysis was performed using GraphPad
769 Prism software. Sample sizes are described in the figure legends.
770
771 **Data availability**

The high-throughput sequencing data generated during this study is being deposited at the NCBI Sequence Read Archive database under PRJNA1288558. Raw data from the genome-wide knockout screen is provided in Supplementary Tables 3–6. Key plasmids from this work will be deposited to Addgene for distribution. Other plasmids and cell lines are available from the corresponding author on request.

Code availability

The code used for analyzing base editing efficiencies are available at https://github.com/pinellolab/CRISPResso2. The code used for analyzing CRISPR screen results are available in Supplementary Note 1 and at https://sourceforge.net/p/mageck/wiki/Home/.

Acknowledgements

This work was supported by the Whitehead Institute and Whitehead Fellows Program (A.R.); NIH Director's Early Independence Award DP5OD037342 (A.R.); Merkin Institute for Transformative Technologies in Healthcare (A.R.); McGuire Family Foundation (A.R.); and the James M. and Cathleen D. Stone Foundation (A.R.). H.J. acknowledges support from the National Research Foundation of Korea. A.S. was supported by the Whitehead Scholars Program at Williams College. We thank H. Keys and the Functional Genomics Platform at Whitehead Institute for providing the genome-wide sgRNA library used in our study; A. Nelson, D. Liu, and the Whitehead Genome Technology Core for access to Illumina sequencing instrumentation; and the Jain, Reddien, Weissman, and Young Labs for generous access to equipment.

Author contributions

A.R. conceived the project. D.L., H.J., A.G., A.S., and A.R. designed the research, performed experiments, and analyzed data. H.J. performed mouse experiments. A.R. wrote the manuscript, and all authors edited the manuscript.

Competing interests

The authors declare competing financial interests: D.L. and A.R. have filed a patent application on this work through the Whitehead Institute. The remaining authors declare no competing interests.

References

1. Raguram, A., Banskota, S. & Liu, D.R. Therapeutic in vivo delivery of gene editing agents. *Cell* **185**, 2806-2827 (2022).
2. van Haasteren, J., Li, J., Scheideler, O.J., Murthy, N. & Schaffer, D.V. The delivery challenge: fulfilling the promise of therapeutic genome editing. *Nat Biotechnol* **38**, 845-855 (2020).
3. Wang, D., Zhang, F. & Gao, G. CRISPR-Based Therapeutic Genome Editing: Strategies and In Vivo Delivery by AAV Vectors. *Cell* **181**, 136-150 (2020).
4. Wei, T. et al. Delivery of Tissue-Targeted Scalpels: Opportunities and Challenges for In Vivo CRISPR/Cas-Based Genome Editing. *ACS Nano* **14**, 9243-9262 (2020).
5. Wang, J.Y. & Doudna, J.A. CRISPR technology: A decade of genome editing is only the beginning. *Science* **379**, eadd8643 (2023).
6. Tsuchida, C.A., Wasko, K.M., Hamilton, J.R. & Doudna, J.A. Targeted nonviral delivery of genome editors in vivo. *Proc Natl Acad Sci U S A* **121**, e2307796121 (2024).
7. An, M. et al. Engineered virus-like particles for transient delivery of prime editor ribonucleoprotein complexes in vivo. *Nat Biotechnol* **42**, 1526-1537 (2024).
8. Banskota, S. et al. Engineered virus-like particles for efficient in vivo delivery of therapeutic proteins. *Cell* **185**, 250-265 e216 (2022).
9. Choi, J.G. et al. Lentivirus pre-packed with Cas9 protein for safer gene editing. *Gene Ther* **23**, 627-633 (2016).
10. Geilenkeuser, J. et al. Engineered nucleocytosolic vehicles for loading of programmable editors. *Cell* **188**, 2637-2655 e2631 (2025).
11. Haldrup, J. et al. Engineered lentivirus-derived nanoparticles (LVNPs) for delivery of CRISPR/Cas ribonucleoprotein complexes supporting base editing, prime editing and in vivo gene modification. *Nucleic Acids Res* **51**, 10059-10074 (2023).
12. Halegua, T. et al. Delivery of Prime editing in human stem cells using pseudoviral NanoScribes particles. *Nat Commun* **16**, 397 (2025).
13. Hamilton, J.R. et al. In vivo human T cell engineering with enveloped delivery vehicles. *Nat Biotechnol* **42**, 1684-1692 (2024).
14. Hamilton, J.R. et al. Targeted delivery of CRISPR-Cas9 and transgenes enables complex immune cell engineering. *Cell Rep* **35**, 109207 (2021).
15. Indikova, I. & Indik, S. Highly efficient 'hit-and-run' genome editing with unconcentrated lentivectors carrying Vpr.Prot.Cas9 protein produced from RRE-containing transcripts. *Nucleic Acids Res* **48**, 8178-8187 (2020).
16. Ling, S. et al. Customizable virus-like particles deliver CRISPR-Cas9 ribonucleoprotein for effective ocular neovascular and Huntington's disease gene therapy. *Nat Nanotechnol* **20**, 543-553 (2025).
17. Lu, Z. et al. Lentiviral Capsid-Mediated Streptococcus pyogenes Cas9 Ribonucleoprotein Delivery for Efficient and Safe Multiplex Genome Editing. *CRISPR J* **4**, 914-928 (2021).
18. Lyu, P., Javidi-Parsijani, P., Atala, A. & Lu, B. Delivering Cas9/sgRNA ribonucleoprotein (RNP) by lentiviral capsid-based bionanoparticles for efficient 'hit-and-run' genome editing. *Nucleic Acids Res* **47**, e99 (2019).

19. Lyu, P. et al. Adenine Base Editor Ribonucleoproteins Delivered by Lentivirus-Like Particles Show High On-Target Base Editing and Undetectable RNA Off-Target Activities. *CRISPR J* **4**, 69-81 (2021).
20. Lyu, P., Wang, L. & Lu, B. Virus-Like Particle Mediated CRISPR/Cas9 Delivery for Efficient and Safe Genome Editing. *Life (Basel)* **10** (2020).
21. Mangeot, P.E. et al. Genome editing in primary cells and in vivo using viral-derived Nanoblades loaded with Cas9-sgRNA ribonucleoproteins. *Nat Commun* **10**, 45 (2019).
22. Raguram, A., An, M., Chen, P.Z. & Liu, D.R. Directed evolution of engineered virus-like particles with improved production and transduction efficiencies. *Nat Biotechnol* (2024).
23. Xu, D. et al. Programmable epigenome editing by transient delivery of CRISPR epigenome editor ribonucleoproteins. *Nat Commun* **16**, 7948 (2025).
24. Lam, B. et al. Multi-species genome-wide CRISPR screens identify conserved suppressors of cold-induced cell death. *eLife* (2024).
25. Replogle, J.M. et al. Combinatorial single-cell CRISPR screens by direct guide RNA capture and targeted sequencing. *Nat Biotechnol* **38**, 954-961 (2020).
26. Seczynska, M., Bloor, S., Cuesta, S.M. & Lehner, P.J. Genome surveillance by HUSH-mediated silencing of intronless mobile elements. *Nature* **601**, 440-445 (2022).
27. Seczynska, M. & Lehner, P.J. The sound of silence: mechanisms and implications of HUSH complex function. *Trends Genet* **39**, 251-267 (2023).
28. DeKelver, R.C. et al. Functional genomics, proteomics, and regulatory DNA analysis in isogenic settings using zinc finger nuclease-driven transgenesis into a safe harbor locus in the human genome. *Genome Res* **20**, 1133-1142 (2010).
29. Liao, J. et al. Therapeutic adenine base editing of human hematopoietic stem cells. *Nat Commun* **14**, 207 (2023).
30. Johnson, S.S., Zhang, C., Fromm, J., Willis, I.M. & Johnson, D.L. Mammalian Maf1 is a negative regulator of transcription by all three nuclear RNA polymerases. *Mol Cell* **26**, 367-379 (2007).
31. Vannini, A. et al. Molecular basis of RNA polymerase III transcription repression by Maf1. *Cell* **143**, 59-70 (2010).
32. Vorlander, M.K. et al. Structural basis for RNA polymerase III transcription repression by Maf1. *Nat Struct Mol Biol* **27**, 229-232 (2020).
33. Musunuru, K. et al. In vivo CRISPR base editing of PCSK9 durably lowers cholesterol in primates. *Nature* **593**, 429-434 (2021).
34. Richter, M.F. et al. Phage-assisted evolution of an adenine base editor with improved Cas domain compatibility and activity. *Nat Biotechnol* **38**, 883-891 (2020).
35. Neugebauer, M.E. et al. Evolution of an adenine base editor into a small, efficient cytosine base editor with low off-target activity. *Nat Biotechnol* **41**, 673-685 (2023).
36. Levy, J.M. et al. Cytosine and adenine base editing of the brain, liver, retina, heart and skeletal muscle of mice via adeno-associated viruses. *Nat Biomed Eng* **4**, 97-110 (2020).
37. Montagna, C. et al. VSV-G-Enveloped Vesicles for Traceless Delivery of CRISPR-Cas9. *Mol Ther Nucleic Acids* **12**, 453-462 (2018).

895 38. O'Driscoll, E.E., Arora, S., Lang, J.F., Davidson, B.L. & Shalem, O. CRISPR screen
896 reveals modifiers of rAAV production including known rAAV infection genes playing
897 an unexpected role in vector production. *Mol Ther Methods Clin Dev* **33**, 101408
898 (2025).
899 39. Barnes, C.R. et al. Genome-wide activation screens to increase adeno-associated
900 virus production. *Mol Ther Nucleic Acids* **26**, 94-103 (2021).
901 40. Iaffaldano, B.J., Marino, M.P. & Reiser, J. CRISPR library screening to develop
902 HEK293-derived cell lines with improved lentiviral vector titers. *Front Genome Ed* **5**,
903 1218328 (2023).
904 41. Kunitake, K. et al. Barcoding of small extracellular vesicles with CRISPR-gRNA
905 enables comprehensive, subpopulation-specific analysis of their biogenesis and
906 release regulators. *Nat Commun* **15**, 9777 (2024).
907 42. Lu, A. et al. Genome-wide interrogation of extracellular vesicle biology using
908 barcoded miRNAs. *Elife* **7** (2018).
909 43. Strebinger, D. et al. Cell type-specific delivery by modular envelope design. *Nat*
910 *Commun* **14**, 5141 (2023).
911 44. Clement, K. et al. CRISPResso2 provides accurate and rapid genome editing
912 sequence analysis. *Nat Biotechnol* **37**, 224-226 (2019).
913 45. Shen, W., Le, S., Li, Y. & Hu, F. SeqKit: A Cross-Platform and Ultrafast Toolkit for
914 FASTA/Q File Manipulation. *PLoS One* **11**, e0163962 (2016).
915 46. Clement, K., Farouni, R., Bauer, D.E. & Pinello, L. AmpUMI: design and analysis of
916 unique molecular identifiers for deep amplicon sequencing. *Bioinformatics* **34**, i202-
917 i210 (2018).
918 47. Langmead, B., Trapnell, C., Pop, M. & Salzberg, S.L. Ultrafast and memory-efficient
919 alignment of short DNA sequences to the human genome. *Genome Biol* **10**, R25
920 (2009).
921 48. Li, W. et al. MAGeCK enables robust identification of essential genes from genome-
922 scale CRISPR/Cas9 knockout screens. *Genome Biol* **15**, 554 (2014).
923